# Spectra of weakly decaying identified particles at 0.9 and 7 TeV with the CMS detector

Krisztián Krajczár[a] for the CMS Collaboration

KFKI RMKI, Budapest, Hungary

**Abstract.** Spectra of strange hadrons have been measured in proton-proton collisions at 0.9 and 7 TeV center-of-mass energies, recorded by the CMS experiment at the CERN Large Hadron Collider. The $K_S^0$, $\Lambda^0, \bar{\Lambda}^0$, and $\Xi^\pm$ particles were reconstructed from their decay topologies and the event yields were measured as a function of the rapidity and the transverse momentum. The measured yields exceed the predictions of current Monte Carlo models.

## 1 Introduction

Measurements of particle yields and spectra are an essential step in understanding proton-proton collisions at the LHC. The CMS Collaboration has, in the first half of 2010, published results on particle spectra of charged particles at 0.9, 2.36 and 7 TeV center-of-mass (c.m.) energies [1, 2]. In the measurement presented here it is repeated for strange mesons and baryons ($K_S^0$, $\Lambda^0$, $\bar{\Lambda}^0$, $\Xi^\pm$). These measurements provide a testing ground for the interplay of soft and hard QCD interactions at the LHC, for the universality of fragmentation models and for the baryon transport mechanism. They also provide valuable information for the tuning of the Monte Carlo (MC) models and are an important tool for the understanding of the tracking system.

Minimum bias collisions at the LHC can be classified as elastic scattering, inelastic single-diffractive dissociation, inelastic double-diffractive dissociation and inelastic non-diffractive scattering. The results presented here refer to non-single-diffractive (NSD) interactions [2], based on collision data recorded by the CMS experiment at 0.9 and 7 TeV. The $K_S^0$, $\Lambda^0$ and $\Xi$ are long-lived particles ($c\tau > 1$ cm) and can be identified from their decay products originating from a displaced secondary vertex. The particles were reconstructed from their decays $K_S^0 \rightarrow \pi^+\pi^-$, $\Lambda^0 \rightarrow p\pi^-$ plus charge conjugate (c.c.), and $\Xi^- \rightarrow \Lambda^0\pi^-$ plus c.c. For each particle species, a comprehensive analysis was performed, which includes: the corrected rapidity, $y$ ($y = 0.5 \ln[(E + p_z)/(E - p_z)]$, where $E$ is the energy and $p_z$ the momentum component in the direction of the colliding protons) and transverse momentum, $p_T$, distributions normalized to NSD events; the average $p_T$, the value $\frac{dN}{dy}|_{y=0}$ and the integrated yield per NSD event for $|y| < 2$. Monte Carlo models and lower energy data were also compared to the results. Unless specified, the results will always refer to each particle and its c.c.

[a] e-mail: `krisztian.krajczar@cern.ch`

## 2 Experimental conditions

The data presented in this paper were collected by the CMS experiment in early spring 2010 from proton-proton collisions at center-of-mass energies of 0.9 and 7 TeV. A detailed description of the CMS detector can be found in [3].

The events were selected online requiring activity in the two beam scintillator counters (BSC, $3.23 < |\eta| < 4.65$), coinciding with colliding proton bunches. Here $\eta$, the pseudorapidity, is defined as $\eta = -\ln \tan(\theta/2)$ and $\theta$ is the polar angle of the direction of the particle with respect to the anti-clockwise beam direction. The offline selection required in addition deposits in each end of the forward calorimeter (HF) [1], for a total energy of at least 3 GeV, selecting preferentially NSD events. A primary vertex (PV) reconstructed in the tracker was required and beam-halo and other beam-related background events were rejected as described in reference [1]. From pp collisions at 0.9 and 7 TeV, 9.05 M and 22.90 M events, respectively, were selected with these criteria. The inelastic pp rate for the running period analyzed was less than 50 Hz, at which rate the pile-up due to two or more minimum-bias collisions occurring in the same bunch crossing is negligible.

Minimum-bias Monte Carlo samples were generated using PYTHIA 8 [4] and PYTHIA 6 [5] with two different parametrizations for the underlying event (tunes D6T [6] and P0 [6]), followed by a full detector simulation based on the GEANT4 program [7]. The strangeness suppression factors in PYTHIA were set to their default values, in particular the suppression factor of strange compared to down quarks was set equal to 0.3.

## 3 Reconstruction of the strange particles

Candidates for long-lived strange neutral particles, were identified by selecting pairs of oppositely charged tracks, fitted to a displaced secondary vertex. The selection criteria were chosen after detailed studies of track and vertex reconstruction optimizing for high efficiency and purity. The
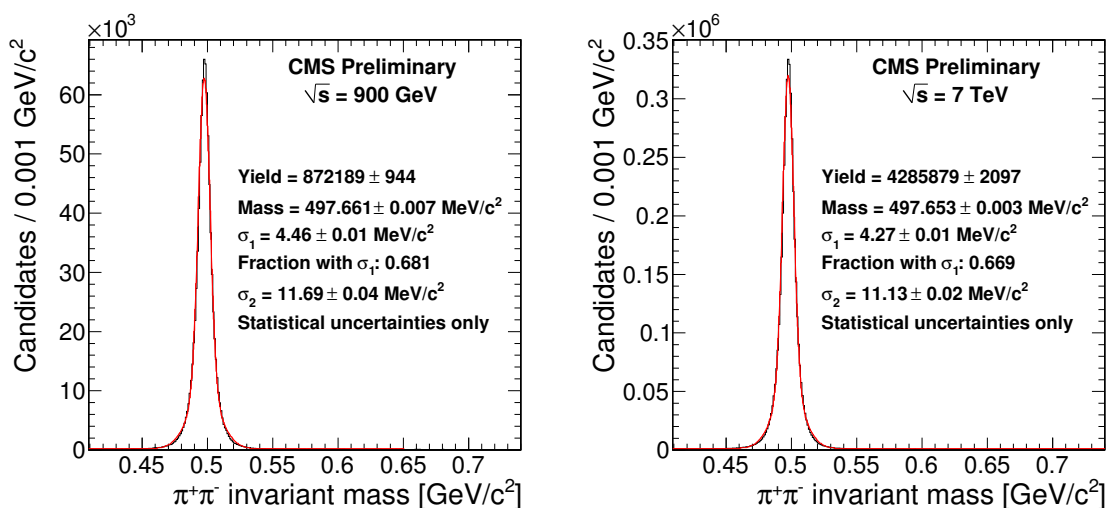
**Fig. 1.** The $\pi^+\pi^-$ invariant mass for the data at 0.9 and 7 TeV. The lines indicate the fit described in the text (for the signal and background) and the yield the number of candidates. The numbers in the legend report only the statistical error.
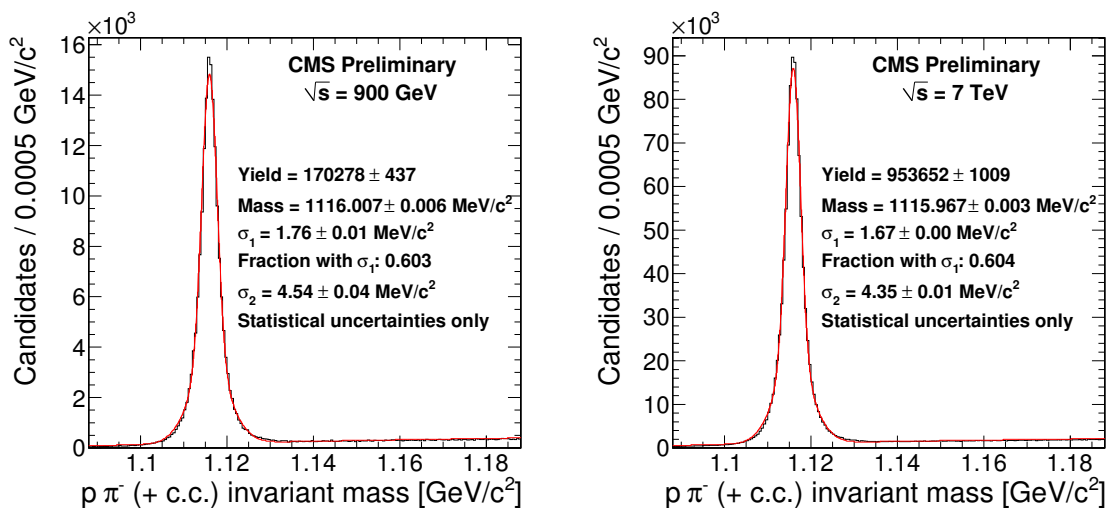


**Fig. 2.** The $p\pi^-$(+c.c) invariant mass for the data at 0.9 and 7 TeV. The lines indicate the fit described in the text and the yield the number of candidates. The numbers in the legend report only the statistical error.

tracks were reconstructed from the inner tracker, requiring a $\chi^2$/ndf for the track fit less than 5. Secondary tracks were selected requiring a distance of closest approach to the PV in 3 dimensions greater than 3 standard deviations ($\sigma$), based on the event-by-event error. The secondary vertex (SV) was also required to be separated by more than $5\sigma$ from the primary vertex, where $\sigma$ included the uncertainty from both the PV and SV. The SV was also required to be located not more than $4\sigma$ further from the PV than the innermost hit of each of the two secondary tracks, to ensure the tracks were consistent with having originated at the reconstructed vertex.

The $K^0_S$ mesons were identified from their decay $K^0_S \rightarrow \pi^+\pi^-$. Both charged particles were assumed to be pions and the invariant mass of each pair was reconstructed. Figure 1 shows the $\pi^+\pi^-$ invariant mass distributions for the two c.m. energies. In order to suppress the contamination

at high $p_T$ due to $\Lambda^0 \rightarrow p\pi^-$ decays, the corresponding invariant mass of the track pair using a $p\pi^-$ hypothesis was required to be 2.5 $\sigma$ greater than the $\Lambda^0$ mass value. Only prompt $K^0_S$ were selected by requiring their momentum vectors to point back to the primary vertex within $3\sigma$. The number of $K^0_S$ candidates was extracted by fitting the data with the sum of a double Gaussian for the signal and a second-order polynomial function for the background.

The $\Lambda^0$ baryons were identified from their decay $\Lambda^0 \rightarrow p\pi^-$, where the charged track with lower momentum was assigned the pion mass. Figure 2 shows the $p\pi^-$ invariant mass distributions for the two c.m. energies. The $\Lambda^0$ particles coming from secondary decays of $\Xi$ and $\Omega^-$ were suppressed by requiring its momentum vector to point back to the primary vertex within $3\sigma$. In order to suppress the contamination due to $K^0_S$, the corresponding invariant mass using a $\pi^-\pi^+$ pair hypothesis was required to be 2.5 $\sigma$ smaller
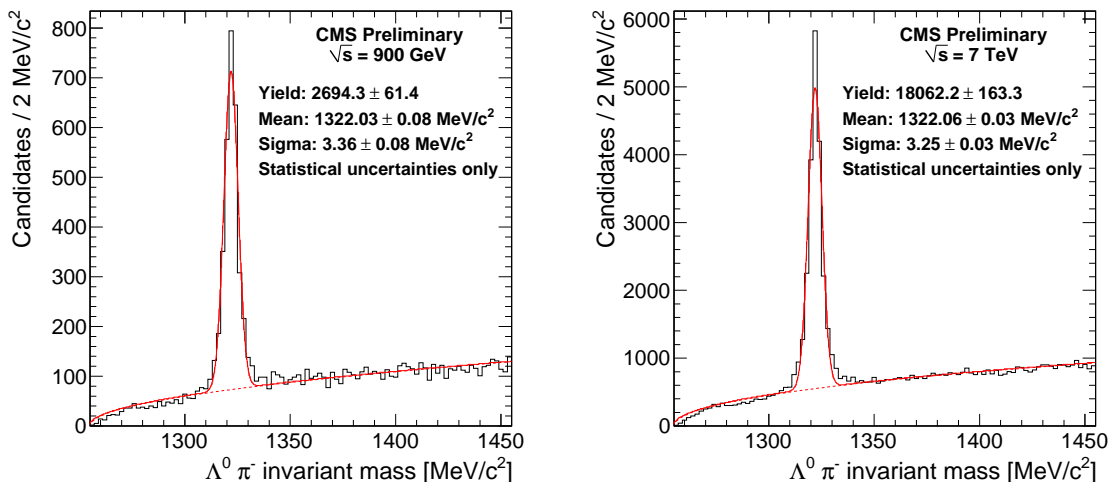
**Fig. 3.** The $\Lambda^0\pi^-$(+c.c.) invariant mass for the data at 0.9 and 7 TeV. The lines indicate the fit described in the text and the yield the number of candidates. The numbers in the legend report only the statistical error.

than the $K_S^0$ mass value. The number of $\Lambda^0$ candidates was extracted by fitting the data with the sum of a double Gaussian for the signal, and a function of the form $Aq^Be^{Cq+Dq^2}$, where $q = m_\Lambda - (m_p + m_\pi)$, for the combinatorial background.

The $\Xi^-$ particles were reconstructed from the decay $\Xi^- \to \Lambda^0\pi^-$. The $\Lambda^0$ candidates were selected as described above, and were combined with a negative track, assumed to be a pion. The three tracks were required to be separated by more than $3\sigma$ from the primary vertex. The $\Lambda^0$ and $\pi^-$ candidate tracks were fit to a common vertex, requiring a fit probability greater than 1%.

The distance between the decay vertex of the $\Xi^-$ and the PV had to be greater than $4\sigma$. Finally, the $\Xi^-$ trajectory was required to point to the PV within $3\sigma$. Only events with exactly one reconstructed $\Xi^-$ were kept. Fig. 3 shows the measured reconstructed mass for the two data samples at 0.9 and 7 TeV. The distributions were fitted with a single Gaussian function for the signal, and an exponential of the form $Ae^{Bq}$, with $q = m_\Xi - (m_\Lambda + m_\pi)$, for the combinatorial background.

The fitted $K_S^0$, $\Lambda^0$ and $\Xi^-$ masses are in good agreement with the Particle Data Group (PDG) [8] values.

## 4 Efficiency corrections

The results of this analysis are presented in terms of three kinematical distributions: the proper decay time, $ct$, the transverse momentum, $p_T$, and the rapidity. In order to minimize the corrections due to the acceptance of the CMS tracker, the strange particles were reconstructed only within $|y| < 2$. The measured $p_T$ range was 0-10 GeV for the $K_S^0$, 0.2-10 GeV for the $\Lambda^0$, and 0.6-6 GeV for the $\Xi^-$.

For each distribution, the signal was extracted using the mass peak fit in each bin of that variable, where the bins were chosen according to the statistics of the sample in each bin. A corrected yield was calculated, taking into account the trigger, selection and reconstruction efficiency, including acceptance effects, and the branching ratio. In the case of the $\Lambda^0$, the MC efficiency factor also corrected for the small remaining contribution of $\Lambda^0$ coming from higher-mass hyperon decays. For the correction factors, the MC simulations with PYTHIA 8 ($K_S^0$ and $\Lambda^0$) and PYTHIA 6 with the D6T tune ($\Xi^-$) were used. The additional P0 tune was used to check systematic errors. The non-prompt $\Lambda$ production was increased by a factor of two in the MC, in order to match the observed $\Lambda$ and $\Xi$ yields in the data (see later in the text). As the trigger used for this analysis preferentially selected NSD events, all distributions were corrected to measure yields from non-single-diffractive interactions.

None of the three PYTHIA samples (PYTHIA 8 or PYTHIA 6 with D6T or P0) accurately reproduces the track multiplicity, therefore each event in the MC was reweighted to reproduce the observed track multiplicity before determining the correction factor. In addition, the MC does not give an accurate description of the kinematics, especially in $p_T$, thus each decay candidate in the MC was reweighted in $p_T$ ($y$) before correcting in $y$ ($p_T$) to match the data. The resulting efficiencies are shown in Fig. 4. The efficiency decreases at large rapidity values and increases steeply as a function of $p_T$, and is slightly larger at 7 TeV with respect to 0.9 TeV. The MC reweighting in $p_T$ was also used for the lifetime efficiency correction.

As the true lifetimes are well known quantities, a measurement of the proper decay time $ct = mL/p$, where $L$ is the three-dimensional decay length, is an important check of the efficiency corrections. The corrected $ct$ distributions for the $K_S^0$, $\Lambda^0$, and $\Xi^-$ are shown for the $\sqrt{s} = 0.9$ and 7 TeV data in Fig. 5. The lines in the figure represent a fit with an exponential function, the slope of which provides the measured lifetimes, $\tau$. The fitted $\tau$ values are in reasonable agreement with the PDG values.
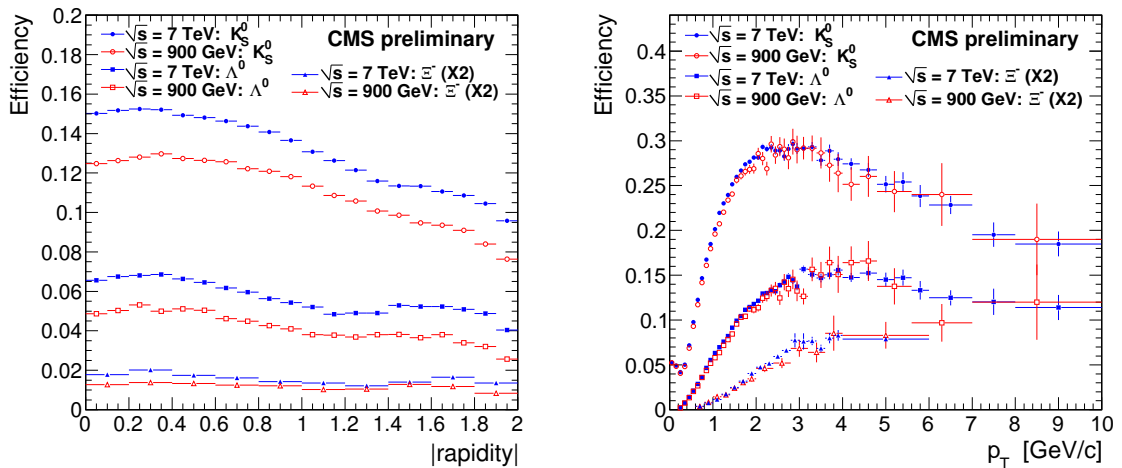
**Fig. 4.** Total reconstruction efficiency as a function of $|y|$ and $p_T$ for $K_S^0$, $\Lambda^0$, and $\Xi^-$ produced promptly in the range $|y| < 2$. The $\Xi^-$ efficiency has been multiplied by two for clarity.



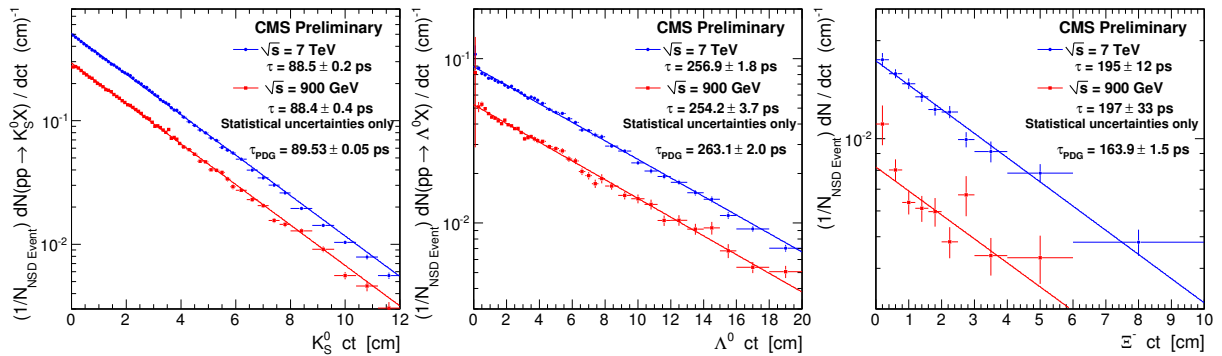**Fig. 5.** $K_S^0$, $\Lambda^0$ and $\Xi^-$ corrected decay time distributions at $\sqrt{s} = 0.9$ and 7 TeV.

## 5 Systematic uncertainties and checks

The systematic uncertainties can be divided in three categories: largely uncorrelated errors affecting the shape of the $p_T$ and $y$ distributions, correlated errors that do not affect the overall normalization, and correlated overall normalization uncertainties.

The following systematic uncertainties affected the shape of the measured distributions (the mean uncertainty is shown in parentheses):

- The MC was changed from PYTHIA 8 to PYTHIA 6 with tunes D6T and P0 (2% for $K_S^0$, 3% for $\Lambda^0$ and $\Xi^-$).
- The event weights for the track multiplicity distribution were calculated for two alternative selections, the first one requiring a PV for at least two reconstructed tracks, the second one without any requirement on the HF deposits (0.5%).
- The MC reweighting was done in two dimensions in $y$ and $p_T$ or a smooth function in $y$ or $p_T$ was used (1%).
- For the $\Lambda^0$, the non-prompt $\Lambda^0$ baryon production in the MC was decreased by a factor of two, corresponding to the default PYTHIA production (2%).

- The vertex significance cuts ($\pm 1\sigma$), the distance of closest approach of the tracks and candidates ($\pm 1\sigma$) and the vertex fit probability (+1%, −0.9%), were varied by the quantities indicated in parentheses (4%).
- The uncertainty on the efficiency of the secondary track reconstruction was taken to be the fractional difference between the measured and the PDG lifetimes (1% for $K_S^0$, 5% for $\Lambda^0$ and 8% for $\Xi^-$).
- The fraction of reconstructed candidates in the MC not originating from true candidates was taken into account (1.0%).

The following systematic uncertainties are correlated bin-to-bin:

- The track reconstruction (2%/track), the misalignment (0.1%/track), and acceptance (1%) uncertainties were evaluated as in our previous analysis [1].
- The rapidity measurements for $\Lambda^0$ and $\Xi^-$ required an extrapolation down to $p_T = 0$ from $p_T = 200$ MeV and 600 MeV, respectively. The extrapolation was computed with two different methods, with a fit function (see Section 6.2) and directly from the MC. The associated

**Table 1.** Systematic uncertainties at 7 TeV on the $y$ distribution. The uncertainties at 0.9 TeV are similar except for the $\Xi^-$ which is much higher (overall sum of 20.1%) due to the $p_T$ extrapolation. Correlated errors include the $p_T$ extrapolation.

| Source | $K_S^0$ | $\Lambda^0$ | $\Xi^-$ |
|---|---|---|---|
| Uncorrelated | 5.8% | 8.9% | 9.5% |
| Correlated | 4.1% | 4.5% | 9.4% |
| Normalization | 4.5% | 4.5% | 4.5% |
| Sum | 8.4% | 11.0% | 14.1% |

systematic uncertainty was taken as half the difference between these two methods (1.8% for $\Lambda^0$ at 7 TeV and up to approximately 16.0% for $\Xi^-$ at 0.9 TeV).

Other normalization uncertainties, related to the trigger, were evaluated as described here:

– The correction to NSD events was evaluated using the PYTHIA 6 with tunes D6T and P0, instead of PYTHIA 8. The fraction of single diffractive events in PYTHIA, still remaining after cuts, was increased by 50% (4.5%).

The following additional checks were performed:

– The corrected event yields were also calculated separately for $y > 0$ and $y < 0$, in order to find possible effects due to incorrect modeling of the asymmetric efficiency of the CMS tracker, and were found consistent within the statistical errors.
– For the $K_S^0$ and $\Lambda^0$, an alternative track [1] and secondary vertex reconstruction algorithm [9] was used to select the candidates in two-dimensional $y$ and $p_T$ bins. The candidates were reconstructed from the tracks with a simple algorithm which applied geometrical cuts on daughter and mother candidates to reduce the combinatorial background. The efficiency of this second method was higher at the price of a lower signal to background ratio. The efficiency correction factors were derived in a two-dimensional grid in $y$ and $p_T$. The corrected yields were found in agreement with the nominal analysis within 1.5$\sigma$ for the $K_S^0$ and within less than 1$\sigma$ for the $\Lambda^0$.

As an example, a summary of the various sources and related effects for the $y$ distribution is given in Table 1.

# 6 Results

## 6.1 Strange particle yields

The results reported here refer to NSD interactions [10]. The NSD raw events were corrected for the trigger efficiency and the fraction of non NSD events after the selection, using the MC simulation. The corrected number of events amounted to 10.1 M for $\sqrt{s} = 0.9$ TeV and 24.5 M for $\sqrt{s} = 7$ TeV.

The corrected $K_S^0$, $\Lambda^0$ and $\Xi^-$ yields are reported, normalized to the number of NSD events, in Fig. 6. The $y$ distributions are relatively flat in the central rapidity range, while slowly decreasing at higher values, especially at $\sqrt{s} = 7$ TeV. They show a steeply falling distribution in $p_T$.

**Table 3.** Results on the average $p_T$. In each column the first uncertainty represents the statistical error, the second the systematics.

| Particle | $\sqrt{s} = 0.9\,TeV$ $< p_T >$ (GeV/c) | $\sqrt{s} = 7\,TeV$ $< p_T >$ (GeV/c) |
|---|---|---|
| $K_S^0$ | $0.657 \pm 0.002 \pm 0.038$ | $0.789 \pm 0.001 \pm 0.046$ |
| $\Lambda^0$ | $0.849 \pm 0.004 \pm 0.076$ | $1.054 \pm 0.003 \pm 0.094$ |
| $\Xi^-$ | $1.00 \pm 0.03 \pm 0.10$ | $1.22 \pm 0.01 \pm 0.12$ |

## 6.2 Analysis of $p_T$ spectrum and yield at $y = 0$

The corrected $p_T$, shown in Fig. 7 spectra were fitted with the Tsallis function [11], as done in our previous publication [1]:

$$\frac{1}{N}\frac{dN}{dp_T} = C p_T \left[ 1 + \frac{\sqrt{p_T^2 + m^2} - m}{nT} \right]^{-n} \quad (1)$$

where $C$ is the normalization parameter and $T$ and $n$ are parameters that control the shape. Table 2 gives the parameters resulting from the Tsallis fit. The average $p_T$ extracted using this function is shown in Table 3. As expected, the average $p_T$ increases with increasing particle mass and with increasing c.m. energy. The results are also compared to previous experiments at lower energies [12–16] and to charged particles [2,17] in Fig. 8.

From the corrected yield, the value at $y = 0$, $\frac{dN}{dy}|_{y=0}$, and the total yield for $|y| < 2$ were extracted. For this purpose, the fitted Tsallis distributions was used to extrapolate the yield down to $p_T = 0$. The results are reported in Table 4. The ratio for $\Lambda^0/K_S^0$ production is $0.54 \pm 0.02$ (stat.) $\pm$ 0.05 (syst.) at $\sqrt{s} = 0.9$ TeV and $0.52 \pm 0.01$ (stat.) $\pm$ 0.05 (syst.) at $\sqrt{s} = 7$ TeV. The ratio for $\Xi^-/\Lambda^0$ production is $0.10 \pm 0.01$ (stat.) $\pm 0.02$ (syst.) at $\sqrt{s} = 0.9$ GeV and $0.13 \pm 0.01$ (stat.) $\pm 0.02$ (syst.) at $\sqrt{s} = 7$ TeV. In these ratios the systematic uncertainty due to the normalization cancels out.

## 6.3 Comparison with PYTHIA

Table 5 shows a comparison of data with the PYTHIA Monte Carlo simulation having D6T tune. This shows several interesting features. First, there is a large increase in the measured production cross section of strange particles as the c.m. energy increases from 0.9 to 7 TeV, which is not modeled by the Monte Carlo. The other noticeable feature is that the deficit in strange particles production as modelled in present MC simulation gets worse as the particle mass and strangeness increase.

These features are also evident in Fig. 6, where the rapidity distribution for data is shown for the three strange particles compared to the PYTHIA samples. None of the samples reproduces the observed rate. It has to be noted that PYTHIA predicts a lower yield for charged particles in general [1,2]. The two MC models the PYTHIA 8 and the PYTHIA 6 with P0 tunes have a dependence on rapidity
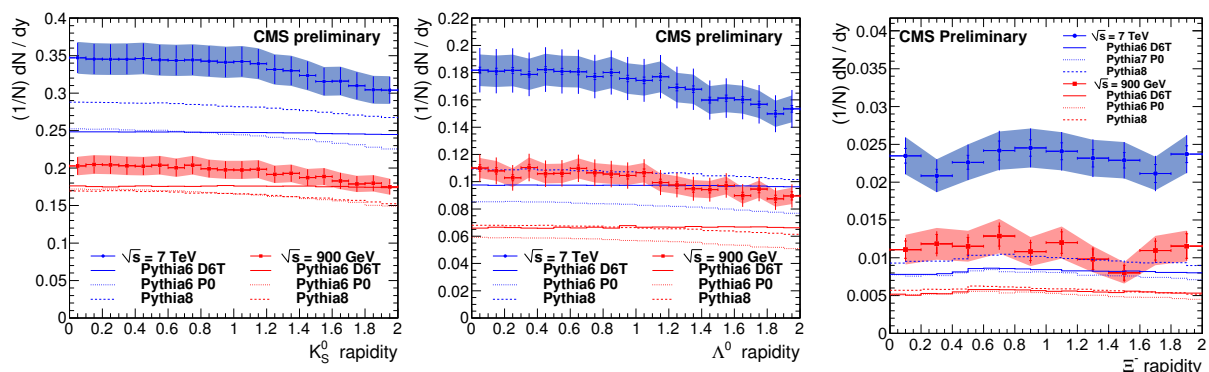
**Fig. 6.** $K_S^0$, $\Lambda^0$ and $\Xi^-$ production per NSD event versus $|y|$. The inner vertical error bars (when visible) show the statistical errors, the outer the statistical and uncorrelated systematic uncertainties summed in quadrature. The overall normalization uncertainty is shown as a band. The solid line is a fit with the Tsallis function as described in the text. Comparisons with three PYTHIA Monte Carlo samples are also shown.
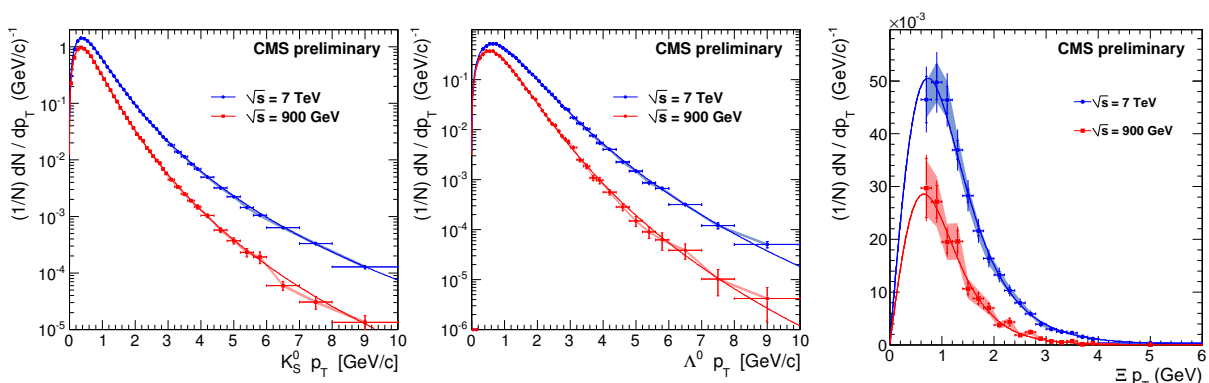


**Fig. 7.** $K_S^0$, $\Lambda^0$ and $\Xi^-$ production per NSD event versus $p_T$. The inner vertical error bars (when visible) show the statistical errors, the outer the statistical and uncorrelated systematic uncertainties summed in quadrature. The overall normalization uncertainty is shown as a band. The solid line is a fit with the Tsallis function as described in the text. Comparisons with three PYTHIA Monte Carlo samples are also shown.

**Table 2.** Results of fits of the Tsallis function to the data. In each column the first uncertainty represents the statistical error, the second the systematics.

| Particle | $\sqrt{s} = 0.9\,TeV$ | | $\sqrt{s} = 7\,TeV$ | |
| | $T$ (GeV) | $n$ | $T$ (GeV) | $n$ |
|---|---|---|---|---|
| $K_S^0$ | $0.187 \pm 0.001 \pm 0.011$ | $7.86 \pm 0.06 \pm 0.46$ | $0.215 \pm 0.001 \pm 0.012$ | $6.79 \pm 0.03 \pm 0.39$ |
| $\Lambda^0$ | $0.218 \pm 0.002 \pm 0.019$ | $9.84 \pm 0.25 \pm 0.88$ | $0.290 \pm 0.002 \pm 0.026$ | $9.28 \pm 0.12 \pm 0.83$ |
| $\Xi^-$ | $0.28 \pm 0.02 \pm 0.03$ | $13.0 \pm 3.1 \pm 1.2$ | $0.34 \pm 0.01 \pm 0.03$ | $9.8 \pm 0.8 \pm 0.9$ |

**Table 4.** $\frac{dN}{dy}|_{y=0}$ and integrated yield $N$ in data for $|y| < 2$. In each column the first uncertainty represents the statistical, the second the systematic error.

| Particle | $\sqrt{s} = 0.9\,TeV$ | | $\sqrt{s} = 7\,TeV$ | |
| | $\frac{dN}{dy}\|_{y=0}$ | $N$ | $\frac{dN}{dy}\|_{y=0}$ | $N$ |
|---|---|---|---|---|
| $K_S^0$ | $0.203 \pm 0.002 \pm 0.017$ | $0.781 \pm 0.002 \pm 0.066$ | $0.347 \pm 0.002 \pm 0.029$ | $1.333 \pm 0.002 \pm 0.112$ |
| $\Lambda^0$ | $0.110 \pm 0.002 \pm 0.012$ | $0.406 \pm 0.004 \pm 0.045$ | $0.182 \pm 0.002 \pm 0.020$ | $0.686 \pm 0.003 \pm 0.075$ |
| $\Xi^-$ | $0.011 \pm 0.001 \pm 0.002$ | $0.038 \pm 0.002 \pm 0.008$ | $0.023 \pm 0.001 \pm 0.003$ | $0.078 \pm 0.001 \pm 0.011$ |

**Table 5.** Comparison between PYTHIA D6T and data. In each column the first uncertainty represents the statistical error, the second the systematics.

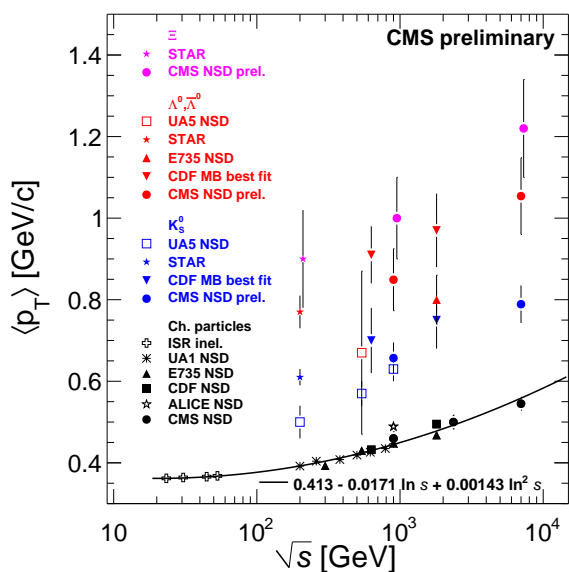| Particle | $\dfrac{\frac{dN}{dy}\mid_{y=0}(7TeV)}{\frac{dN}{dy}\mid_{y=0}(0.9TeV)}$ | | $\dfrac{\frac{dN}{dy}\mid_{y=0}(\text{PYTHIA D6T})}{\frac{dN}{dy}\mid_{y=0}(\text{Data})}$ | |
| --- | --- | --- | --- | --- |
| | Data | PYTHIA D6T | 0.9 TeV | 7 TeV |
| $K^0_S$ | $1.71 \pm 0.02 \pm 0.20$ | $1.41$ | $0.87 \pm 0.01 \pm 0.07$ | $0.72 \pm 0.01 \pm 0.06$ |
| $\Lambda^0$ | $1.65 \pm 0.04 \pm 0.26$ | $1.48$ | $0.60 \pm 0.01 \pm 0.07$ | $0.54 \pm 0.01 \pm 0.06$ |
| $\Xi^-$ | $2.09 \pm 0.09 \pm 0.27$ | $1.47$ | $0.48 \pm 0.05 \pm 0.09$ | $0.33 \pm 0.02 \pm 0.05$ |



**Fig. 8.** Average $p_T$ for charged hadrons, $K^0_S$, $\Lambda^0$ and $\Xi^-$, as a function of the center-of-mass energy. The CMS measurements are for $|y| < 2$. Also shown are the most recent results from UA5 (p$\bar{\text{p}}$ for $|y| < 2.5$ at $\sqrt{s} = 546$ GeV and $|y| < 3.5$ at $\sqrt{s} = 200, 900$ GeV), E735 (p$\bar{\text{p}}$ for $-0.36 < \eta < 1.0$), CDF (p$\bar{\text{p}}$ for $|\eta| < 1.0$) and STAR (pp for $|y| < 0.5$). The $\Xi^-$ points have been sligthly displaced horizontally for better visibility. The vertical bars indicate the statistical and systematic errors summed in quadrature.

that better reproduces the shape of the data. The $p_T$ distribution in PYTHIA also has a different shape compared to the data, however, after averaging over $p_T$, the values are quite close at 7 TeV, and a bit lower at 0.9 TeV.

# 7 Summary

This paper presents a first study of strange particles production at the LHC, at the highest center-of-mass energy ever reached. The results show an increase in the production rate of strange particles not yet simulated correctly in the current tunes of PYTHIA. The discrepancy gets larger at higher c.m. energy and for higher mass and strangeness.

# References

1. CMS Collaboration, JHEP **1002**, (2010) 041
2. CMS Collaboration, Phys. Rev. Lett. **105**, (2010) 022002
3. CMS Collaboration, JINST **3**, (2008) S08004
4. T. Sjöstrand, S. Mrenna and P. Skands, Comput. Phys. Commun. **178**, (2008) 852-867
5. T. Sjöstrand, S. Mrenna and P. Skands, JHEP **05**, (2006) 026
6. P. Bartalini, (ed.) and L. Fano, (ed.), DESY-PROC-2009-06
7. T. Agostinelli et al., Nucl. Instr. Meth. **A 506**, (2003) 250
8. C. Amlset et al., Phys. Lett. **B 667**, (2008) 1
9. F. Sikler, Nucl. Instrum. Meth. **A 621**, (2010) 526
10. CMS Collaboration, CMS-PAS-QCD-10-007
11. C. Tsallis, J. Stat. Phys. **52**, (1988) 479
12. UA5 Collaboration, Nucl. Phys. **B 258**, (1985) 505
13. UA5 Collaboration, Phys. Lett. **B 199**, (1987) 311
14. E735 Collaboration, Phys. Rev. Lett. **62**, (1989) 12
15. CDF Collaboration, Phys. Rev. **D 72**, (2005) 052001
16. STAR Collaboration, Phys. Rev. **C 75**, (2007) 064901
17. ALICE Collaboration, Phys. Lett. **B 693**, (2010) 53